DOI: 10.1021/ma9015399

Macromolecules
ARTICLE

Dilute Solution Properties and Surface Attachment of RAFT Polymerized 2-Vinyl-4,4-dimethyl Azlactone (VDMA)

Bradley S. Lokitz,*,† Jamie M. Messman,‡ Juan Pablo Hinestrosa,§ José Alonzo,∥ Rafael Verduzco,‡ Rebecca H. Brown,⊥ Masashi Osa,‡,# John F. Ankner,† and S. Michael Kilbey II‡,×

†*Spallation Neutron Source, Oak Ridge National Laboratory, One Bethel Valley Road, Oak Ridge, Tennessee 37831,* ‡*Center for Nanophase Materials Sciences, Oak Ridge National Laboratory, One Bethel Valley Road, Oak Ridge, Tennessee 37831,* §*Department of Chemical and Biomolecular Engineering, Clemson University, Clemson, South Carolina 29634-0909,* ∥*Chemical Sciences Division, Oak Ridge National Laboratory, One Bethel Valley Road, Oak Ridge, Tennessee 37831,* ⊥*Department of Chemistry, Virginia Polytechnic Institute and State University, Blacksburg, Virginia 24061,* #*Department of Polymer Chemistry, Kyoto University, Kyoto, Japan 615-8510, and* ×*Department of Chemistry, University of Tennessee, Knoxville, Tennessee 37996*

Received July 15, 2009; Revised Manuscript Received October 14, 2009

ABSTRACT: We report the controlled radical polymerization of 2-vinyl-4,4-dimethyl azlactone (VDMA), a 2-alkenyl-2-oxazolin-5-one monomer that contains a polymerizable vinyl moiety and a highly reactive, pendant azlactone, as well as dilute solution properties and surface attachment and functionalization. Reversible addition−fragmentation chain transfer (RAFT) was used to polymerize VDMA in benzene at 65 °C using either 2-(2-cyanopropyl) dithiobenzoate (CPDB) or 2-dodecylsulfanylthiocarbonylsulfanyl-2-methylpropionic acid (DMP) as RAFT chain transfer agents (CTAs). The pseudo-first-order kinetics and resultant well-defined polymers of low polydispersity indicate that both CTAs afford control over the RAFT polymerization of VDMA. Dynamic and static light scattering and small-angle neutron scattering (SANS) were performed to determine the weight-average molecular weight, radius of gyration, and second virial coefficient of VDMA homopolymers in THF. Additionally, well-defined polymers of VDMA containing carboxyl end groups were covalently attached to epoxy-modified silicon wafers via esterification to produce polymeric scaffolds that can be subsequently functionalized for various bio-inspired applications.

Introduction

Polymers from reactive monomers such as those based on active esters,[1,2] epoxides,[3] anhydrides,[4] isocyanates,[5] and oxazolones[6] continue to garner a great deal of interest due to their potential application in a variety of biotechnology fields.[7,8] One active monomer with particularly interesting potential is 2-vinyl-4,4-dimethyl azlactone (VDMA) due to its polymerizable vinyl moiety and highly reactive, pendant azlactone funtionality.[9,10] The azlactone moiety of VDMA readily reacts with amines, alcohols, and thiols under relatively mild conditions, providing a facile route to monomer/polymer modification.[6,11] Heilmann and co-workers at 3M performed much of the early work pertaining to VDMA and VDMA-containing polymers, resulting in over 100 patents.[6] With the advent of controlled radical polymerization techniques a renewed interest in VDMA has emerged.[12−14]

Controlled radical polymerization techniques facilitate the synthesis of well-defined polymers with predetermined molecular weights and narrow molecular weight distributions.[15,16] The controlled polymerization of VDMA by reversible addition−fragmentation chain transfer (RAFT),[12] nitroxide-mediated polymerization (NMP),[14] and atom transfer radical polymerization (ATRP)[13] have been independently reported by the groups of Schilli, Grubbs, and Fournier, respectively. More recently Cullen and co-workers used surface-initiated ATRP to graft PVDMA chains on silicon substrates as a means to develop three-dimensional polymer scaffolds for RNase attachment.[8]

Of the controlled radical polymerization techniques, RAFT is arguably the most versatile controlled polymerization method due to its ability to mediate the polymerization of most vinyl monomers and to be carried out under a variety of reaction conditions.[17−20] RAFT also enables polymers with reactive chain ends to be made using functional chain transfer agents (CTAs).[21] These functional CTAs can be used for subsequent chain end modification or end-tethering chains to surfaces. An appealing aspect of this "grafting to" approach is that it allows for polymer molecular weight and polydispersity to be characterized before surface attachment. Surface-anchored polymers, in particular polymer brushes, can be utilized as three-dimensional scaffolds and are emerging as leading candidates for immobilization of biomolecules due to their mechanical stability and high surface area.[8,22−25]

Herein we report the controlled RAFT polymerization of VDMA and the use of these well-defined VDMA homopolymers to provide the first detailed investigation of the dilute solution properties by static and dynamic light scattering and small-angle neutron scattering. In addition, we present a facile strategy for creating bio-inspired surfaces through the immobilization and functionalization of PVDMA.

Experimental Section

Materials. Benzyl chloride (ReagentPlus, 99%), calcium hydride, ethyl acetate (anhydrous, 99.8%), hexanes (CHROMASOLV Plus, for HPLC, ≥98.5%), methanol

*To whom correspondence should be addressed. E-mail: lokitzbs@ornl.gov.

 Published on Web 11/02/2009

(Reagent Plus, ≥99%), potassium ferricyanide (ReagentPlus, ~99%), sodium methoxide (technical, ~30% in methanol), sulfur (reagent grade, powder, purified by sublimation, ~100 mesh), tetrahydrofuran (anhydrous, ≥99.9%, contains 250 ppm BHT as inhibitor), and N_α,N_α-bis(carboxymethyl)-L-lysine hydrate (purum, ≥97.0%), were purchased from Aldrich and used as received. Benzene (ReagentPlus, thiophene free, ≥99%; Aldrich) was dried with calcium hydride, distilled at reduced pressure, and stored over nitrogen. 2,2′-Azobis(2-methylpropionitrile) (AIBN; 98%, Aldrich) was recrystallized from anhydrous methanol at least three times, dried in vacuo, and stored under a blanket of dry nitrogen at 3 °C. 2-Vinyl-4,4-dimethyl azlactone (VDMA; Isochem North America, LLC) was fractionally distilled under reduced pressure, and the middle fraction (~70%) was reserved for use. Silicon wafers (diced to 1 cm × 1.2 cm) were purchased from Silicon Quest. All other reagents were purchased from Aldrich and used as received unless noted otherwise.

Instrumentation. *NMR.* Solution ^{1}H and ^{13}C NMR spectroscopy was performed on a Varian VNMRS 500 MHz multinuclear spectrometer. Samples were placed in 5 mm o.d. tubes with sample concentrations of 5 and 10% (w/v), respectively. Chloroform-*d* ($CDCl_3$) was used as the solvent, and residual solvent peaks serve as internal standards.

Size Exclusion Chromatography (*SEC*). Molecular weights and polydispersities were obtained by SEC using a Waters Alliance 2695 separations module equipped with three Polymer Laboratories PLgel 5 μm mixed-C columns (300 × 7.5 mm) in series, a Waters model 2414 refractive index detector (λ = 880 nm), a Waters model 2996 photodiode array detector, a Wyatt Technology miniDAWN multiangle light scattering (MALS) detector (λ = 660 nm), and a Wyatt Technology ViscoStar viscometer. THF was used as the mobile phase at a flow rate of 1 mL/min.

Off-Line Measurements of Refractive Index Increment (dn/dc). A Wyatt Technology Optilab rEX refractive index detector (λ = 658 nm) was used in conjunction with a Harvard Apparatus PHD 2000 Infusion syringe pump to determine the off-line dn/dc values. Solutions of various concentrations ranging from nominally 0.2 to 2 wt % were prepared and allowed to equilibrate for several days prior to measurement; dn/dc values were calculated using Astra V software.

Light Scattering. Dynamic (DLS) and static (SLS) light scattering experiments were performed using an ALV/DLS/SLS-5000 light scattering system equipped with ALV-5000 multiple tau digital correlator. Vertically polarized light (λ = 632.8 nm) from a JDS Uniphase model 1145P He−Ne gas laser was used as the incident source, and the intensity of the scattered light was measured with no analyzer. For the calibration, the intensity of the scattered light from pure toluene was measured as the reference material. The Rayleigh ratio measured for pure toluene without an analyzer was 1.37 × 10^{-5} cm^{-1} at 25 °C. The most concentrated solution of each sample was prepared gravimetrically and stirred continuously for several days until it appeared homogeneous. All solutions were filtered through a Teflon membrane having a pore size 0.1 μm, and solutions of lower concentration were obtained by successive dilution. The scattered light intensities were measured for each solution and for the pure solvent at scattering angles θ ranging from 28° to 146°. The excess Rayleigh ratio ΔR_θ of each solution over that of the solvent then was calculated from the scattered intensities of the solution and the solvent. A Berry plot was used to analyze the average intensity data.[26] Additionally, DLS measurements were used to determine the diffusion coefficients of the PVDMA samples. The normalized autocorrelation function $g^{(2)}(t)$ of scattered light intensity $I(t)$, where $g^{(2)}(t) = \langle I(0)I(t)\rangle/\langle I(0)\rangle^2$, was measured at scattering angles θ ranging from 28° to 146°. The apparent diffusion coefficient D_{app} was determined by the method of cumulants at each scattering angle.[27] The "true" *z*-average diffusion coefficient $\langle D\rangle_z$ is obtained by extrapolation of D_{app} to a scattering vector of zero (q = 0). In this limit polymer segment fluctuations and other nondiffusional processes no longer contribute to the correlation function obtained by dynamic light scattering.[28] Finally, the hydrodynamic radius, R_H, was calculated from the Stokes−Einstein relation, $R_H = k_B T/6\pi\eta_0 D$, where k_B is the Boltzmann constant, T is the absolute temperature, and η_0 is the solvent viscosity. A value of η_0 = 0.465 cP for THF at 25 °C was used.

Small-Angle Neutron Scattering (*SANS*). SANS measurements were performed on the NG-3 SANS instrument at the NIST Center for Neutron Research. The wavelength of the incident neutron beam was set at 6.0 Å with a wavelength resolution, $\Delta\lambda/\lambda$, of 15%, and the corresponding wavevector, Q, ranged from 0.02 to 0.45 $Å^{-1}$ at three different sample-to-detector distances. The samples were contained in quartz cells having a 1 mm path length, and all measurements were carried out at room temperature. The measured intensity was corrected for detector background and sensitivity and for scattering from the empty cells and placed on an absolute scale using a direct beam measurement.[29]

Ellipsometry. Samples were washed, sonicated, and dried with nitrogen after each surface attachment prior to measuring the film thicknesses using a J.A. Woollam M-2000U variable angle spectroscopic ellipsometer over a wavelength range of 245−999 nm. Thicknesses reported are the average of measurements made from at least three spots on the polymer-modified wafer. To fit the ellipsometric data, each polymer layer was represented as a slab of uniform thickness with sharp interfaces having optical properties described by a Cauchy model (refractive index smoothly varying with wavelength) assuming that the PGMA and PVDMA layers had refractive indices of 1.50 and 1.52 at 632 nm.

Fourier Transform Infrared Spectroscopy (*FTIR*). Transmission spectra were obtained using a Bruker Optics Vertex 70 instrument with a KBr beamsplitter and DTGS detector. Attenuated total reflectance (ATR-FTIR) spectra were obtained using a Harrick Scientific GATR accessory, which has a germanium hemisphere internal reflection element. The samples were placed on the ATR crystal, and intimate contact was obtained by applying 56 in-oz. of torque. A background (256 scans at 4 cm^{-1} resolution) of the clean ATR crystal was used as the reference spectrum. An aperture setting of 6 mm and a scanner velocity of 10 kHz were used. The Fourier transform parameters used are as follows: apodization function of Blackman-Harris 3-Term; phase resolution of 32 cm^{-1}; phase correction mode of Mertz; zero filling factor of 2. The acquisition parameters used were a mode of double-sided, forward−backward and 256 scans at a resolution of 4 cm^{-1}.

Contact Angle. The sessile water contact angles were measured on a Ráme-Hart goniometer (100-00, Mountain Lakes, NJ) using deionized water as the probe liquid. Substrates were rinsed with methanol and deionized water and dried under a stream of nitrogen before measurement. The contact angle for each sample was independently measured at three different locations and averaged.

Atomic Force Microscopy (*AFM*). AFM images were collected using a Veeco Instruments Nanoscope IIIa multimode atomic force microscope. The topographical height and phase contrast images were acquired in tapping mode using a constant amplitude set point. Images were single flattened to correct for tilt and bow effects of the scanner. Images were collected at a scan rate of 0.5 Hz and 512 lines per sample. An antimony (n) doped silicon tip having a nomimal resonant frequency of 320 kHz and a nominal spring constant of 42 N/m was used.

Neutron Reflectivity (*NR*). Measurements were made using the Liquids Reflectometer (LR) of the Spallation Neutron Source (SNS) at Oak Ridge National Laboratory. The SNS-LR collects specular reflectivity data in a continuous wavelength band at several different incident angles. For the data presented

Scheme 1. RAFT Polymerization of VDMA Using CPDB or DMP with AIBN in Benzene at 65 °C

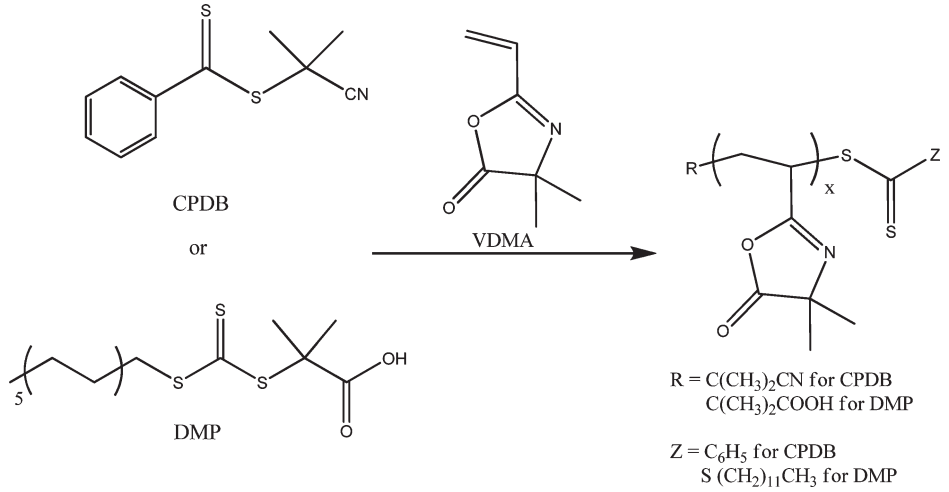

here we used the wavelength band 2 Å $< \lambda <$ 5.5 Å and measured reflectivity at angles θ = 0.15°, 0.25°, 0.40°, 0.70°, 1.20°, 2.20°, and 3.30°, thereby spanning a total wavevector transfer ($Q = 4\pi \sin\theta/\lambda$) range of 0.006 Å$^{-1} < Q <$ 0.360 Å^{-1}. Data were collected at each angle with incident-beam slits set to maintain a constant wavevector resolution of $\delta Q/Q$ = 0.05, which allows the data obtained at six different angles to be stitched together into a single reflectivity curve. To fit the data, the initial thicknesses measured using spectroscopic ellipsometry were used for reflectivity simulations, and then these thicknesses were adjusted to correspond to the superlattice peaks in the neutron reflectivity. The neutron scattering length density, Σ, was determined using the equation $\Sigma = b/V$, where b is the monomer scattering length (sum of scattering lengths of constituent atomic nuclei) and V is the monomer volume. The calculated reflectivity curves were optimized for goodness of fit.[30]

Synthetic Procedures. *RAFT CTA Synthesis*. The RAFT CTA, 2-(2-cyanopropyl) dithiobenzoate (CPDB), was synthesized using a combination of methods published by Mitsukami et al.[31] and Perrier et al.[32] In particular, the RAFT CTA precursors dithiobenzoic acid (DTBA) and di(thiobenzoyl) disulfide were synthesized by Mitsukami's method; CPDB was generated by the reaction of AIBN and di(thiobenzoyl) disulfide and rigorously purified using Perrier's technique. 2-Dodecylsulfanylthiocarbonylsulfanyl-2-methylpropionic acid (DMP) was prepared according to previously reported methods.[21,33]

General RAFT Polymerization. Reactions were formulated in a single-neck 50 mL air-free round-bottom reaction flask equipped with a Teflon-coated magnetic stir bar. In a typical reaction, VDMA (4.17 g, 3.01 $\times$ 10^{-2} mol) was combined with CPDB (12.32 mg, 5.57 $\times$ 10^{-5} mol; VDMA:CPDB = 539), AIBN (1.83 mg; molar ratio of CPDB:AIBN = 5:1) and benzene (30.0 mL). The reaction vessel was capped with a rubber septum, and the solution was sparged with dry argon for ~30 min. The reaction vessel was then placed in a heated oil bath thermostated at 65 °C and allowed to react for a predetermined time, after which the reaction vessel was immersed in liquid nitrogen to quench the polymerization. The RAFT-mediated polymerizations using different CTAs were performed using analogous protocols.

Surface Modification. Silicon samples were cleaned immediately before use by immersion for 90 min in a piranha acid solution at 110 °C (3:1 v/v solution of sulfuric acid (EMD, 95−98%) and 30% hydrogen peroxide (VWR, 29−32%)) followed by rinsing with copious amounts of distilled, deionized water and drying with a stream of dry nitrogen. *Caution: piranha acid should be handled with extreme care, as it reacts violently with most organic materials*.

The attachment procedure originally developed by Luzinov et al., which used an epoxy functionalized "base layer" of poly(glycidyl methacrylate) (PGMA) (M_n = 24 600 g/mol; PDI = 1.61)[34] and carboxylic acid-terminated polymers, was modified to create PVDMA brushes.[35,36] Briefly, silicon wafers were spin-coated (Laurell WS-400B-6NPP/LITE) with a 0.25 wt % solution of PGMA in chloroform, spun at 2500 rpm for 15 s, and immediately annealed for 18 h in an oven preheated to 110 °C. After the PGMA-modified wafers cooled to room temperature, they were immersed in MEK, sonicated for 1 h to remove any unattached PGMA from the surface of the wafer, and then dried with a stream of dry, filtered N_2. Solutions of end-functionalized (carboxy-terminated) PVDMA in chloroform were spun at 2500 rpm for 15 s and immediately annealed for 18 h in an oven preheated to 110 °C to promote the esterification reaction between the COOH on the chain ends and the surface-tethered epoxides. After the PVDMA-modified wafers cooled to room temperature, they were immersed in MEK, sonicated for 30 min to remove any unattached PVDMA from the surface of the wafer, and then dried with a stream of dry, filtered N_2.

Brush Functionalization. PVDMA brushes on silicon wafers were exposed to an 0.1 M aqueous solution of N_α,N_α-bis-(carboxymethyl)-L-lysine hydrate (lysine hydrate) at pH 5. After 48 h the surfaces were removed and washed repeatedly with H_2O followed by sonication to remove unreacted lysine hydrate and dried under a flow of filtered N_2.

Results and Discussion

Polymerization of VDMA via RAFT. Through judicious selection of CTA, solvent, and a free radical source, most vinyl monomers can by polymerized via RAFT. 2-(2-Cyanopropyl) dithiobenzoate (CPDB) has been shown previously to be very effective in the RAFT polymerization of styrenic, (meth)acrylate, and (meth)acrylamido monomers.[37] Recently, Schilli et al. used CPDB to mediate the RAFT polymerization of the reactive monomer VDMA.[12] DMP is a trithiocarbonate that has also been employed to control the polymerization of several vinyl monomers[33] and is of particular interest due to its straightforward synthesis.[21] Building on the preliminary report by Schilli et al. and to prepare well-defined PVMDA for subsequent solution property measurements and surface grafting studies, analogous RAFT polymerizations of VDMA using CPDB and DMP, as illustrated in Scheme 1, were investigated.

Polymerizations were conducted in benzene, and the resultant polymers were isolated by precipitation into cold hexanes. The polymers were further purified by redissolving

them in THF followed by precipitation into hexanes; this process was performed a total of three times to ensure removal of any unreacted monomer. Isolated polymers were dried in vacuo and analyzed via ^{1}H NMR and SEC. The dn/dc value for PVDMA (M_w = 4100 g/mol, PDI = 1.01) determined online was 0.084 mL/g, which was in agreement with the value determined off-line (0.0835 mL/g). A typical ^{1}H NMR spectrum for PVDMA mediated by CPDB is shown in Figure 1. The phenyl protons of the CPDB chain end are clearly visible at 7.38, 7.56, and 7.95 ppm.

Shown in Figure 2a is the pseudo-first-order kinetic plot for the RAFT-mediated polymerization of VDMA in benzene at 65 °C. Pseudo-first-order kinetics are observed for both CTAs, and the apparent rate of polymerization is slightly higher when DMP is used as the CTA. The observed difference in the polymerization rate for the DMP-mediated system is most likely the result of a higher rate of fragmentation from the intermediate radical species.[38] As shown in Figure 2b, the observed M_n as a function of conversion for both CTAs are in good agreement with the theoretical molecular weights (solid line). Additionally, the polydispersity index (PDI) versus conversion for the CPDB- and DMP-mediated RAFT polymerizations of VDMA indicates that both CTAs lead to polymers with narrow PDIs. Given the pseudo-first-order kinetics, the low PDIs, and the linear increase in molecular weight with conversion, it is clear that both CTAs result in the controlled polymerization of VDMA.

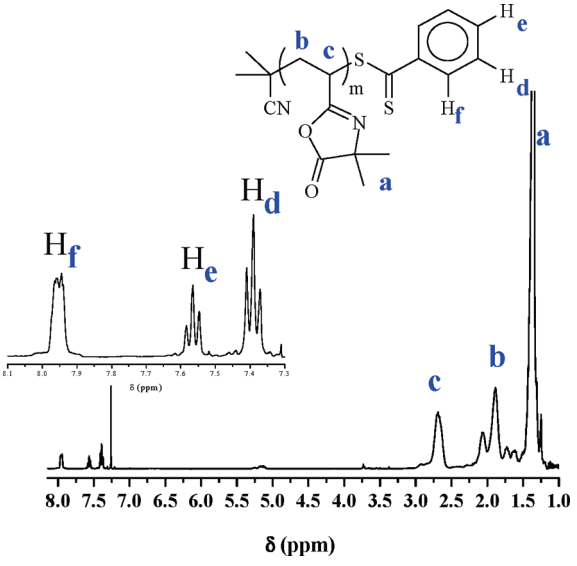

Figure 1. ^{1}H NMR spectrum of PVDMA prepared via RAFT using CPDB as the CTA.

Light Scattering Measurments of PVDMA. To the best of our knowledge there are no reports of the dilute solution properties of PVDMA. Therefore, static and dynamic light scattering measurements were used to gain insight into the conformations, interactions, and transport properties of PVDMA. SLS measurements were carried out in THF at 25 °C to determine the weight-average molecular weight, M_w, radius of gyration, R_g, and second virial coefficient, A_2, of two different PVDMA samples identified as entries A and B in Table 1. The measured dn/dc values of 0.0835 and 0.0820 cm^3/g for entry A (Table 1) and entry B (Table 1), respectively, were used in the analyses of the SLS data. Differences between dn/dc values measured at 632.8 nm and those measured off-line at 658 nm were assumed to be negligible; this is supported by the fact that the dn/dc values determined for PVDMA synthesized by free radical polymerization and calculated based on 100% mass recovery agreed with those measured at 658 nm.[11]

In parts a and b of Figure 3, Berry plots are constructed for entries A and B (Table 1) by plotting the values of $(Kc/\Delta R_\theta)^{1/2}$ against $q^2 + 3c$ and $q^2 + 5c$, respectively. The unfilled circles represent the data obtained at finite concentrations and at finite scattering angles. Extrapolation of these data yielded the limiting values of $(Kc/\Delta R_\theta)^{1/2}$ at $c = 0$ (represented by the filled circles) and $q = 0$ (represented by the filled triangles).

The M_w values obtained by SLS closely agree with those obtained by SEC-MALS, and positive A_2 values indicate that THF is a good solvent for PVDMA. For each of the samples, the lines formed by $\lim_{c\to 0}(Kc/\Delta R_\theta)^{1/2}$ as a function of q^2 (filled circles) are nearly horizontal, meaning that values of R_g cannot be determined with high accuracy. However, by using SANS, R_g for a dilute solution of PVDMA in THF (Figure 4) could be determined. The SANS data shows a

Table 1. Summary of Results Obtained by Static and Dynamic Light Scattering from PVDMA Solutions in THF

entry	M_w (kg/mol)	A_2 (cm^3 mol g^{-2}) × 10^4	D_z (cm^2 s^{-1}) × 10^6	R_H (nm)
A	5.9 ± 0.04	6.78 ± 0.26	3.61 ± 0.34	1.3 ± 0.13
B	25.2 ± 0.02	5.78 ± 0.06	1.54 ± 0.03	3.6 ± 0.06

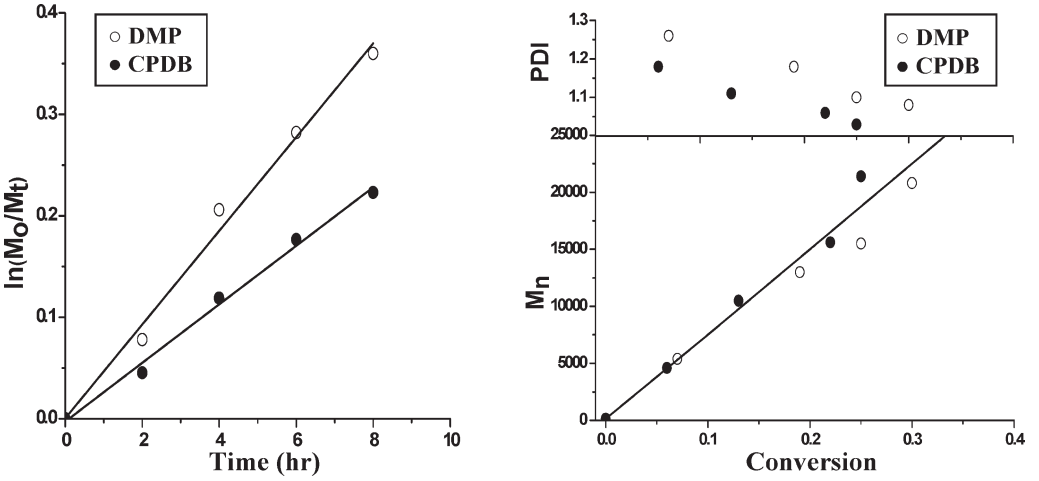

Figure 2. (a) Pseudo-first-order kinetic plot and (b) M_n and PDI versus conversion for the CPDB- and DMP-mediated polymerizations of VDMA at 65 °C in benzene.

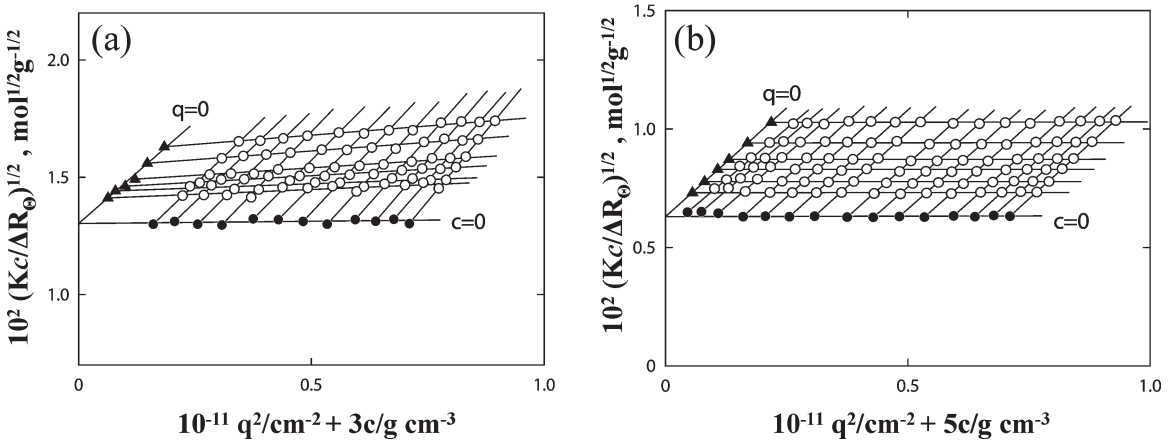

Figure 3. Square-root plots for PVDMA in THF at 25 °C: (a) M_w = 5.89 kg/mol, (b) M_w = 25.2 kg/mol.

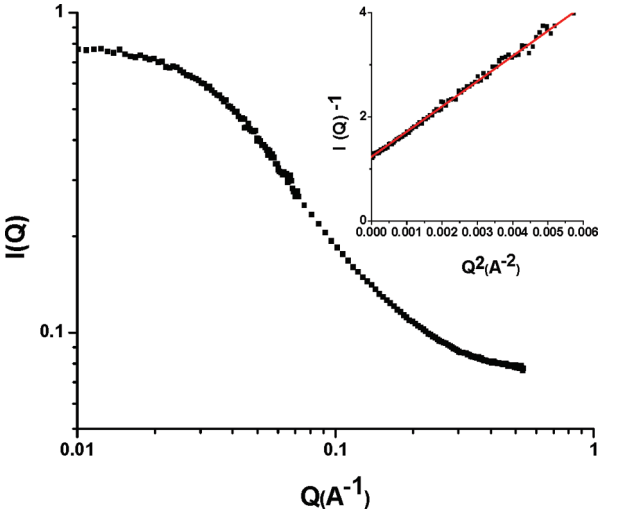

Figure 4. SANS data and Zimm plot (inset) for 2 wt % PVDMA (M_w = 25.2 kg/mol) in THF at 25 °C.

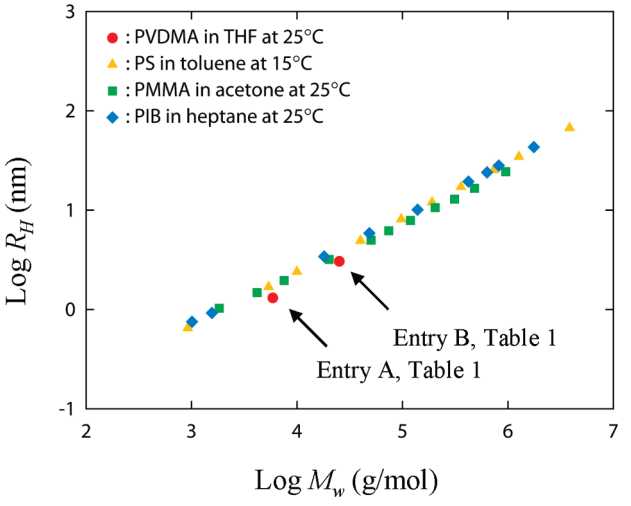

Figure 5. Comparison of R_H as a function of molecular weight for PVDMA (this work) with other flexible polymers.

plateau in the low-q region, indicating that the PVDMA chains are well-solvated, and a Zimm plot (Figure 4 inset) of the data gives a value of 3.3 nm for the 25.2 kg/mol PVDMA in a dilute d-THF solution.

Values of z-average translational diffusion coefficients obtained using DLS measurements are also given in Table 1 along with hydrodynamic radii, R_H, values calculated using the Stokes−Einstein relationship. Since we are aware of no other dilute solution characterizations of PVDMA, in Figure 5 we overlay (M_w, R_H) data pairs obtained by light scattering measurements of PVDMA in THF onto an extensive set of analogous data obtained for other well-known flexible polymer/good solvent systems. These comparisons indicate that PVDMA in THF behaves similarly to other flexible polymers in good solvents.[39−41]

Surface Attachment and Functionalization. Tethering premade polymer chains by one end to a surface to create a polymer "brush" is advantageous because it allows the polymer chains to be fully characterized prior to surface attachment and the grafting density to be readily calculated.[22,42] Silicon surfaces bearing epoxide groups were prepared using the approach described in the Experimental Section, which is represented in Scheme 2, and described initially by Luzinov and co-workers,[35,36] who reported that ~40% of the epoxy groups of PGMA are retained after deposition and annealing. After spin-coating, annealing, and sonication in pure solvent the thickness of the resultant epoxy-bearing polymer layer is, on average, 6.8 nm as measured by ellipsometry.

Carboxylic acid-terminated VDMA polymers synthesized using DMP and having different molecular weights were spin-coated onto epoxide surfaces and allowed to react for 18 h at 110 °C under vacuum. At elevated temperatures, carboxylic acid groups are able to react with the epoxy groups of PGMA.[35,43] A negative control experiment using PVDMA without a terminal carboxylic acid group was also carried out. This PVDMA was spin-coated onto a PGMA base layer and annealed. After sonicating the surface for 30 min and rinsing with copious amounts of solvent, the overall film thickness changed by ~0.1 nm, which indicates that the reaction between the epoxy groups of PGMA and the azlactone of PVDMA is insignificant. However, when carboxylic acid-terminated PVDMA is used, the overall surface thickness increases by 6 to 8 nm, depending on the molecular weight and concentration of the PVDMA solution. The results from the surface attachment experiments are summarized in Table 2 and are comparable to results reported by Luzinov and co-workers for polystyrene brushes of similar molecular weight.[36,44] The measured thickness were used along with eq 1 to determine the grafting density of chains, σ, on each surface.

$$\sigma = (h\rho N_a)/M_n \quad (1)$$

Scheme 2. Schematic of the Procedures Used To Create Polymer Brush-Functionalized Silicon Surfaces[a]

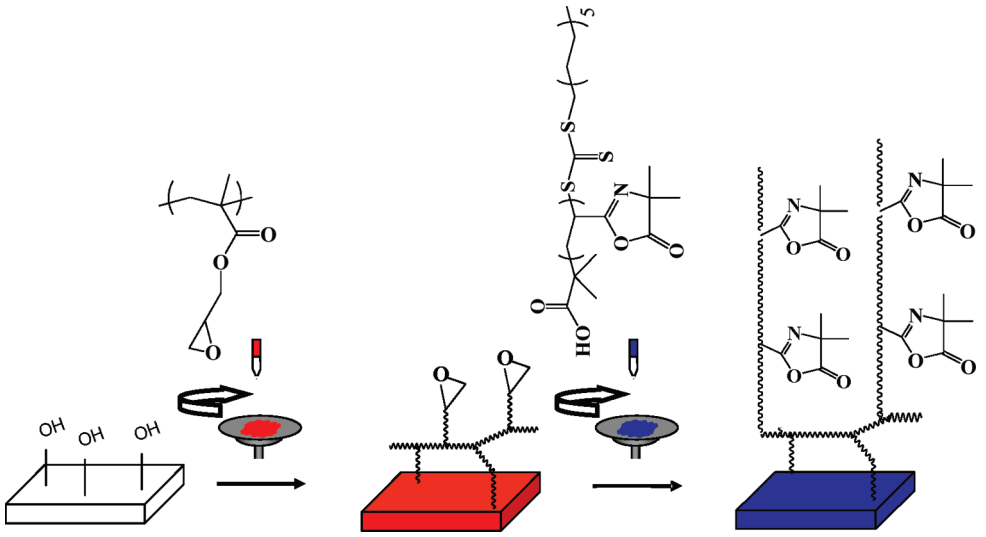

[a] Solutions were spin-coated at 2500 rpm and annealed at 110 °C for 18 h.

Table 2. Summary of PVDMA Brush Thickness, Grafting Density, and Distance between Tethering Points

entry	M_n (g/mol)	concentration (wt %)[a]	PVDMA brush layer thickness (nm)[b,c]	R_g (nm)[d]	σ (chains/nm^2)	D (nm)	$D/2R_g$[e]
1	8 900	0.14	6.0	1.8	0.40	1.8	0.50
2	8 900	0.50	8.0	1.8	0.54	1.5	0.42
3	18 900	0.29	7.8	2.9	0.25	2.3	0.40
4	18 900	0.50	7.1	2.9	0.23	2.4	0.41
5	32 500	0.50	6.3	4.0	0.12	3.3	0.41

[a] The concentrations of entries 1, 3, and 5 were selected to make the number of polymer chains constant (9.6×10^{-7} mol) for the different M_n samples. [b] The PGMA base layer had an average thickness of 68 Å. [c] The reported thickness is the average from multiple measurements made on three different surfaces prepared under identical conditions. [d] R_g was calculated using $R_g = bN^{3/5}$ with $b = 0.15$ nm.[45] [e] A value of $D/2R_g < 1$ indicates that the chains are crowded and brushes are formed.[48]

In this expression, h is the dry brush layer thickness, ρ is the bulk density of the brush layer (~1.05 g/cm^3), N_a is Avogadro's number, and M_n (g/mol) is the number-average molecular weight. The average distance between tethering points, D, is calculated by assuming that the projected area of each chain on the surface is circular: $D = 2(\pi\sigma)^{-1/2}$. To determine whether the tethered PVDMA chains are crowded and overlapping when solvated, the R_g for each of the brushes was first approximated using the relationship between R_g and degree of polymerization, N: $R_g = bN^{3/5}$. Here b is the characteristic segment size, and the exponent value of 3/5 is assumed for a polymer in a good solvent.[45] The R_g of 3.3 nm determined by SANS for entry B, Table 1 is used to calculate $b = 0.15$ nm for PVDMA in THF. This value is then used to estimate the R_g of the brushes. In each case, and as shown in Table 2, $D/2R_g < 1$, indicating that the solvated chains stretch away from the surface and the grafted PVDMA layers reside in the brush regime.[22,46−48]

Shown in Figure 6 is a plot of σ versus M_n for entries 1, 3, and 5 in which the number of polymer chains is kept constant to a first approximation by controlling the concentration and amount of polymer solution applied to the surface prior to spin-coating. We note that the layer thickness measured after annealing and sonication is greater than $2R_g$ (calculated based on a good solvent, not melt conditions) in all cases except entry 5, indicating that chains from greater than R_g above the surface are diffusing and attaching to the PGMA layer during the long annealing time (18 h). Additionally, the grafting density achieved for the PVDMA brushes is well below the maximum density of available epoxy groups in the PGMA layer that was calculated by Iyer et al.,[35] suggesting that maximum surface coverage is not reached. Although it is

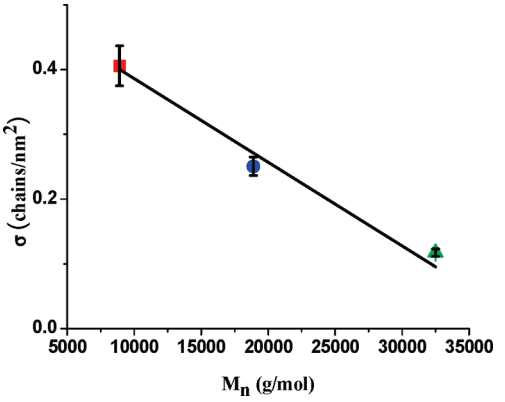

Figure 6. Grafting density versus number-average molecular weight (M_n) for PVDMA brushes with M_n = 8900 (red square), 18 900 (blue circle), and 32 500 (green triangle). PVDMA concentrations were selected to keep the number of polymer chains constant (to a first approximation).

difficult to draw a direct conclusion on the effect of the number of available chains on the grafting density, the salient outcome is that the results follow the well-known relationship expressed by eq 1 reflecting the fact that the grafting density decreases linearly with increasing molecular weight.[48]

An attractive feature of PVDMA is the ability of the azlactone to react rapidly with primary amines.[6] We have recently reported the functionalization of VDMA and PVDMA[11] and surface-confined PVDMA[34] with various primary amine-containing compounds. In this report, we utilize this facile functionalization strategy as proof-of-concept for creating bio-inspired surfaces. Specifically,

PVDMA brushes (entry 3, Table 2) were exposed to an aqueous solution of N_α,N_α-bis(carboxymethyl)-L-lysine hydrate (lysine hydrate) for 48 h. Lysine hydrate, which has a single primary amine, is of interest because of its ability to bind histidine-tagged proteins when complexed with certain metals via metal-ion affinity interactions.[49] To characterize the changes during functionalizations, the water contact angles for the base layer, brush layer, and functionalized brush layer were measured. PGMA and PVDMA have similar water contact angles of 57° and 53°, respectively. After functionalization with lysine hydrate the water contact angle decreased to 44°. The surface was then exposed to a solution at pH = 9 to deprotonate the carboxylic acid groups; after rinsing the surface with DI water and drying the surface with nitrogen the tethered, lysine-hydrate functionalized PVDMA brush is completely wet by water. The surface layer was then exposed to a solution at pH = 3 and the contact angle returned to 45°. This change was completely reproducible.

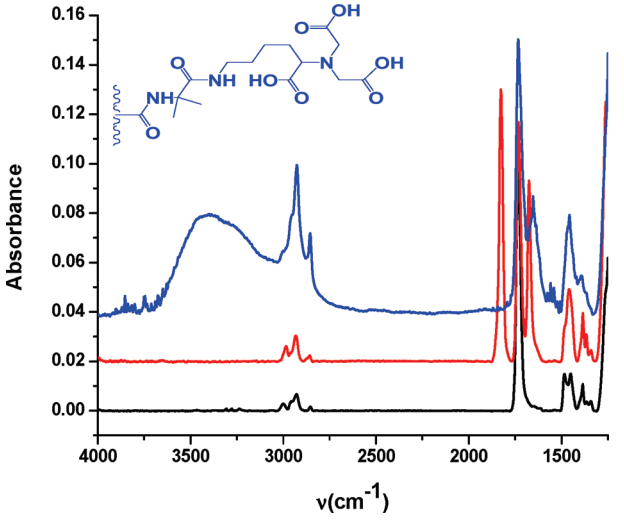

Figure 7. ATR-FTIR spectrum for PGMA (black), PVDMA brushes (red), and N_α,N_α-bis(carboxymethyl)-L-lysine hydrate-functionalized PVDMA brushes (blue). Inset shows proposed structure of N_α,N_α-bis(carboxymethyl)-L-lysine hydrate-functionalized PVDMA brushes.

To further confirm the presence of the expected chemical groups and the success of the attachment strategy, the modified silicon surfaces were characterized using ATR-FTIR spectroscopy. Figure 7 shows the ATR-FTIR spectra for the PGMA base layer (black spectrum), the PVDMA brush layer (red spectrum), and the lysine hydrate-functionalized brush layer (blue spectrum). The presence of the expected bond stretches confirms the presence of the polymer on the surface and its subsequent functionalization. The carbonyl peak for the PGMA primer layer is present at 1720 cm^{-1}, confirming the presence of the base layer.[34] After reacting PVDMA onto the surface, characteristic peaks at 1690 and 1825 cm^{-1} attributed to the PVDMA imine and carbonyl, respectively, are observed.[11,34] The disappearance of the carbonyl peak due to the VDMA and the appearance of peaks at 1680 cm^{-1} for the amide and between 3000 and 3600 cm^{-1} for the carboxylic acids of lysine hydrate indicate that the brushes have been successfully functionalized. Efforts to investigate the binding capabilities and capacities of the functionalized brushes are currently underway, and this will be the focus of a future publication.

The topologies of the surfaces were imaged using atomic force microscopy (AFM), and the results are shown in Figure 8. The height images show molecularly smooth layers throughout the sequence of the PGMA layer attachment, PVDMA brush formation, and subsequent functionalization with lysine hydrate. The height scales are in good agreement with the thicknesses measured with ellipsometry, and the phase images indicate uniformly and densely covered surfaces without significant differences in material hardness. The overall film thickness after functionalization with lysine hydrate increased by 1.5 nm, which is consistent with thickness changes observed for other functionalized brush systems reported in the literature.[24]

Neutron reflectivity data for one of the PVDMA-modified surfaces are presented in Figure 9. In Figure 9a, the reflectivity (R) is plotted as a function of wavevector transfer, Q. The reflectivity profile (light blue squares) shows prominent

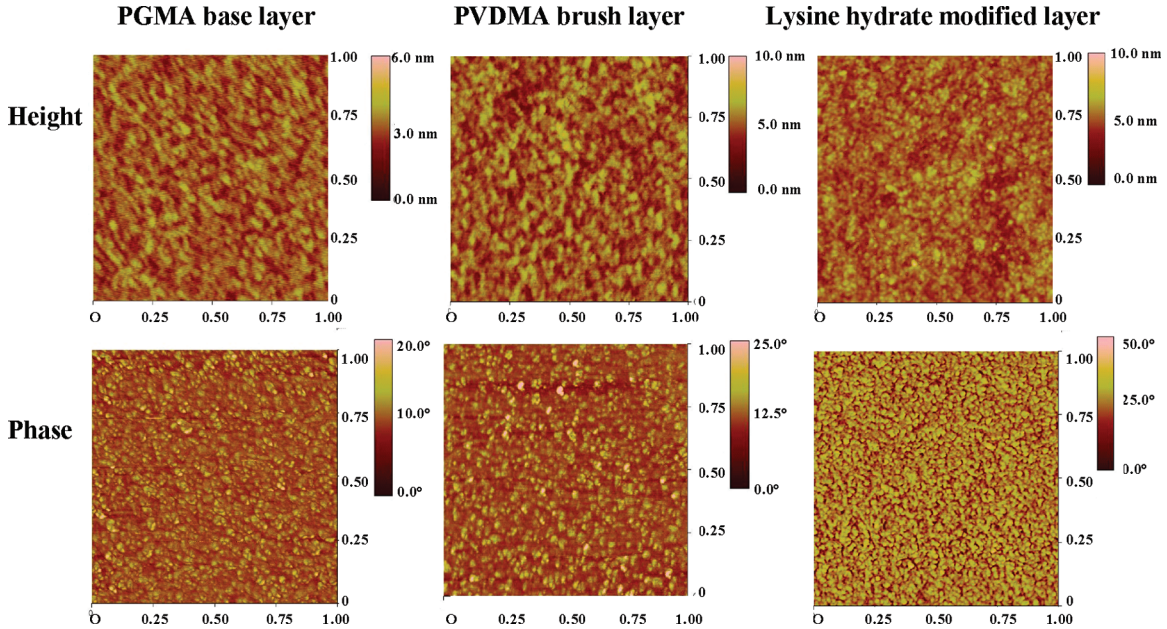

Figure 8. AFM height and phase images for regions 1 μm × 1 μm in size for a PGMA-modified surface, PVDMA brush layer (atop PGMA), and the lysine hydrate-modified PVDMA layer. These images were acquired for the sample identified as entry 3 of Table 2.

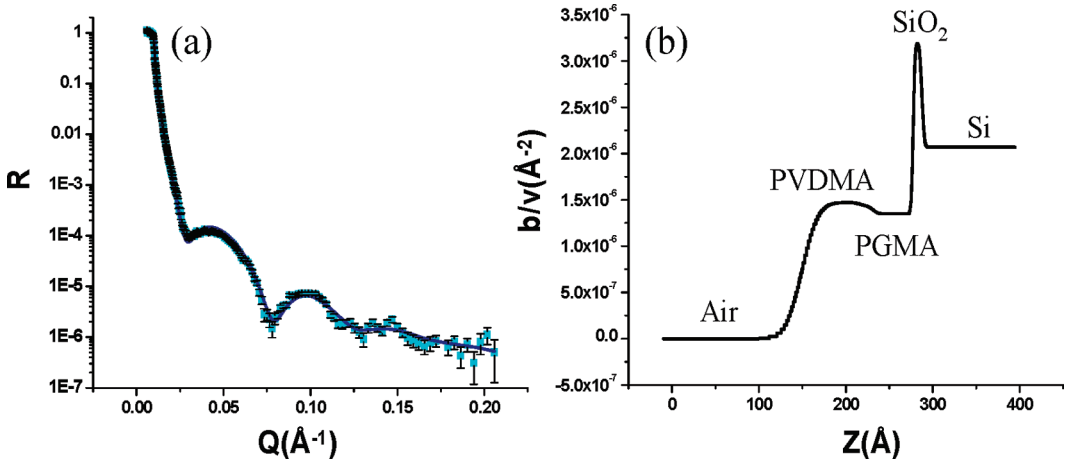

Figure 9. (a) Reflectivity as a function of wavevector transfer, Q. The data are shown as solid squares and the model as a dark blue line. (b) Scattering length density profile as a function of thickness, Z, used to generate the model curve.

interference fringes that are captured using a model (dark line) comprised of two distinct polymer layers separated by an interphase layer, which is comprised of a mixture of the PVDMA brush and the PGMA base layer. This slab−interphase−slab representation is based on the model proposed by Luzinov and co-workers for a polystyrene brush layer grafted onto PGMA in which the interphase layer was calculated to be 1.5−1.8 nm thick.[35] Agreement between the model and the data is achieved using a PVDMA layer thickness of 6.8 nm, an interphase thickness of 1.4 nm, and a PGMA base layer thickness of 4.6 nm. The thickness of the PVDMA layer and the combined thickness of the PGMA base layer and interphase layer are in agreement with values measured by ellipsometry, which are 7.1 and 6.2 nm, respectively. The value for the scattering length density, SLD, of PVDMA was set to 1.47×10^{-6} Å^{-2}, which is consistent with the SLD measured for a thick (500 nm) PVDMA film. The PGMA base layer has an SLD of 1.35×10^{-6} Å^{-2}, which is higher than the SLD calculated based on the molecular composition and an assumed bulk density of 1.05 g/cm^3 (1.20×10^{-6} Å^{-2}). The interphase layer has an intermediate SLD of 1.43×10^{-6} Å^{-2}, which is consistent with model that envisions the interphase layer to be a mixture of the base layer and the tethered brush chains. This three-layer model is represented by the SLD profile shown in Figure 9b, which reflects the proposed structure consisting of a PVDMA brush layer anchored onto a PGMA base layer.

Conclusions

We demonstrate the ability of CPDB and DMP to control the polymerization of VDMA and provide the first report of the dilute solution properties of PVDMA. Well-defined polymers synthesized using DMP provide a way to end-tether PVDMA onto epoxy-modified silicon surfaces via esterification reactions. Using the molecular weight of the PVDMA polymer and the thickness of grafted layer, the grafting densities determined indicate that the tethered PVDMA chains exist in the brush regime, and those reactive brush layers can be functionalized in a facile manner using lysine hydrate. Efforts to further characterize the bio-inspired surface and to exploit the attractive features of VDMA are currently under investigation in our laboratories and will be the subject of future reports.

Acknowledgment. This research was conducted at the Center for Nanophase Materials Sciences and Spallation Neutron Source, which are sponsored at Oak Ridge National Laboratory by the Scientific User Facilities Division, U.S. Department of Energy, (under contract DE-AC05-00OR22725), and enabled through ORNL's Laboratory Directed Research and Development Program, Project No. D07-138. We acknowledge the support of the National Institute of Standards and Technology, U.S. Department of Commerce, in providing the neutron research facilities for the SANS used in this work. Jim Browning and Candice Halbert of ORNL are acknowledged for their help with reflectivity measurements.

References and Notes

(1) Theato, P.; Kim, J.-U.; Lee, J.-C. *Macromolecules* **2004**, *37*, 5475–5478.
(2) Theato, P. *J. Polym. Sci., Part A: Polym. Chem.* **2008**, *46*, 6677–6687.
(3) Xu, F. J.; Li, Y. L.; Kang, E. T.; Neoh, K. G. *Biomacromolecules* **2005**, *6*, 1759–1768.
(4) Beyer, D.; Paulus, W.; Steitz, M.; Maxein, G.; Ringsdorf, H.; Eich, M. *Thin Solid Films* **1995**, *271*, 73–83.
(5) Dorr, M.; Zentel, R.; Dietrich, R.; Meerholz, K.; Brauchle, C.; Wichern, J.; Zippel, S.; Boldt, P. *Macromolecules* **1998**, *31*, 1454–1465.
(6) Heilmann, S. M.; Rasmussen, J. K.; Krepski, L. R. *J. Polym. Sci., Part A: Polym. Chem.* **2001**, *39*, 3655–3677.
(7) Gauthier, M. A.; Gibson, M. I.; Klok, H. A. *Angew. Chem., Int. Ed.* **2009**, *48*, 48–58.
(8) Cullen, S. P.; Liu, X.; Mandel, I. C.; Himpsel, F. J.; Gopalan, P. *Langmuir* **2008**, *24*, 913–920.
(9) Iwakura, Y.; Toda, F.; Torii, Y. *Tetrahedron* **1967**, *23*, 3363–3373.
(10) Stanek, L. G.; Heilmann, S. M.; Gleason, W. B. *Carbohydr. Polym.* **2006**, *65*, 552–556.
(11) Messman, J. M.; Lokitz, B. S.; Pickel, J. M.; Kilbey, S. M. *Macromolecules* **2009**, *42*, 3933–3941.
(12) Schilli, C. M.; Muller, A. H. E.; Rizzardo, E.; Thang, S. H.; Chong, Y. K. *Adv. Controlled/Living Radical Polym.* **2003**, *854*, 603–618.
(13) Fournier, D.; Pascual, S.; Fontaine, L. *Macromolecules* **2004**, *37*, 330–335.
(14) Tully, D. C.; Roberts, M. J.; Geierstanger, B. H.; Grubbs, R. B. *Macromolecules* **2003**, *36*, 4302–4308.
(15) Matyjaszewski, K. *Controlled/Living Radical Polym. Prog. ATRP, NMP, RAFT* **2000**, *768*.
(16) Matyjaszewski, K. *Adv. Controlled/Living Radical Polym.* **2003**, *854*.
(17) Le, T.; Moad, G.; Rizzardo, E.; Thang, S. H. WO 9801478, **1998**.
(18) Rizzardo, E.; Thang, S. H.; Moad, G. WO 9905099, **1999**.
(19) Moad, G.; Rizzardo, E.; Thang, S. H. *Aust. J. Chem.* **2005**, *58*, 379–410.
(20) Lowe, A. B.; McCormick, C. L. *Prog. Polym. Sci.* **2007**, *32*, 283–351.
(21) Gondi, S. R.; Vogt, A. P.; Sumerlin, B. S. *Macromolecules* **2007**, *40*, 474–481.
(22) Zhao, B.; Brittain, W. J. *Prog. Polym. Sci.* **2000**, *25*, 677–710.
(23) Jain, P.; Baker, G. L.; Bruening, M. L. *Annu. Rev. Anal. Chem.* **2009**, *2*, 387–402.
(24) Murata, H.; Prucker, O.; Ruhe, J. *Macromolecules* **2007**, *40*, 5497–5503.

(25) Wang, J.; Gibson, M. I.; Barbey, R.; Xiao, S. J.; Klok, H. A. *Macromol. Rapid Commun.* **2009**, *30*, 845–850.
(26) Berry, G. C. *J. Chem. Phys.* **1966**, *44*, 4550–4564.
(27) Koppel, D. E. *J. Chem. Phys.* **1972**, *57*, 4814–4820.
(28) Schartl, W. *Light Scattering from Polymer Solutions and Nanoparticle Dispersions*; Springer: Berlin, 2007.
(29) Kline, S. R. *J. Appl. Crystallogr.* **2006**, *39*, 895–900.
(30) Ankner, J. F.; Majkrzak, C. F. In *Neutron Optical Devices and Applications*; Proceedings of the International Society for Optical Engineering, San Diego, CA, July 22−24, 1992; Majkrzak, C. F., Wood, J. L., Eds.; International Society for Optical Engineering: Washington, DC, 1992; pp 260−269.
(31) Mitsukami, Y.; Donovan, M. S.; Lowe, A. B.; McCormick, C. L. *Macromolecules* **2001**, *34*, 2248–2256.
(32) Perrier, S.; Barner-Kowollik, C.; Quinn, J. F.; Vana, P.; Davis, T. P. *Macromolecules* **2002**, *35*, 8300–8306.
(33) Lai, J. T.; Filla, D.; Shea, R. *Macromolecules* **2002**, *35*, 6754–6756.
(34) Barringer, J. E.; Messman, J. M.; Banaszek, A. L.; Meyer, H. M.; Kilbey, S. M. *Langmuir* **2009**, *25*, 262–268.
(35) Iyer, K. S.; Zdyrko, B.; Malz, H.; Pionteck, J.; Luzinov, I. *Macromolecules* **2003**, *36*, 6519–6526.
(36) Zdyrko, B.; Varshney, S. K.; Luzinov, I. *Langmuir* **2004**, *20*, 6727–6735.
(37) Moad, G.; Rizzardo, E.; Thang, S. H. *Acc. Chem. Res.* **2008**, *41*, 1133–1142.
(38) Thomas, D. B.; Convertine, A. J.; Hester, R. D.; Lowe, A. B.; McCormick, C. L. *Macromolecules* **2004**, *37*, 1735–1741.
(39) Arai, T.; Abe, F.; Yoshizaki, T.; Einaga, Y.; Yamakawa, H. *Macromolecules* **1995**, *28*, 3609–3616.
(40) Arai, T.; Sawatari, N.; Yoshizaki, T.; Einaga, Y.; Yamakawa, H. *Macromolecules* **1996**, *29*, 2309–2314.
(41) Osa, M.; Abe, F.; Yoshizaki, T.; Einaga, Y.; Yamakawa, H. *Macromolecules* **1996**, *29*, 2302–2308.
(42) Ranjan, R.; Brittain, W. J. *Macromol. Rapid Commun.* **2008**, *29*, 1104–1110.
(43) Koning, C.; Van Duin, M.; Pagnoulle, C.; Jerome, R. *Prog. Polym. Sci.* **1998**, *23*, 707–757.
(44) Iyer, K. S.; Luzinov, I. *Macromolecules* **2004**, *37*, 9538–9545.
(45) Burchard, W. *Adv. Polym. Sci.* **1999**, *143*, 113–194.
(46) Ostaci, R. V.; Damiron, D.; Capponi, S.; Vignaud, G.; Leger, L.; Grohens, Y.; Drockenmuller, E. *Langmuir* **2008**, *24*, 2732–2738.
(47) deGennes, P. G. *Macromolecules* **1980**, *13*, 1069–1075.
(48) Kilbey, S. M.; Watanabe, H.; Tirrell, M. *Macromolecules* **2001**, *34*, 5249–5259.
(49) Sun, L.; Dai, J. H.; Baker, G. L.; Bruening, M. L. *Chem. Mater.* **2006**, *18*, 4033–4039.